A Tuned Microwave Resonator on Flexible Substrate for Nondestructive Water Content Sensing in Fruits

Sen Bing, *Member, IEEE*, Khengdauliu Chawang, *Graduate Student Member, IEEE*, and Jung-Chih Chiao, *Fellow, IEEE*

***Abstract*—This work aims to develop a planar microwave sensor fabricated on a flexible polyimide substrate to monitor the water content of fruits nondestructively. The sensor is based on a planar loop resonator tuned with a concentric metal pad that features improved resonance, compact size, and flexibility to conform to the curved surface of the fruit. The sensing mechanism is to detect electromagnetic resonance that is susceptible to dielectric property changes by water content variations. The robust resonance provides electric fields that penetrate deeper into the fruit tissues, compared with an untuned one, with a sufficient spectral resolution to reach high sensitivity. Experiments were conducted, including long-term continuous water content monitoring and total water content measurements. The sensors demonstrated clear frequency shifting trends when fresh apples became dehydrated, and their initial resonant frequencies indicated total water contents. Simulations were conducted to examine measurement discrepancies induced by inhomogeneous water evaporation and surface curvatures. The feasibility of sensing the watercore defects inside apples was demonstrated with simulations. In addition, the sensor was used to demonstrate the feasibility of measuring water content in potatoes. The promising results show the great potential of the noninvasive and continuous water-content sensor applications in agriculture to study the growth, maturity, anomaly, and storage of fruits and in food processing applications to achieve optimal quality.**

***Index Terms*—Agriculture, food quality, loop resonator, nondestructive, tuning, water content.**

I. Introduction

WATER is a vital factor for the growth and maturation of fruits such as apples. Water constitutes approximately 82%–86% in an apple's composition [1], [2]. The water content in fruits profoundly influences their texture, taste, and overall quality. Particularly, the water content inherent in fruits can vary depending on growth conditions and ripeness. For example, water content may decrease with the fruits' gradually ripening [3], [4]. Dry matter (DM) is a commonly used maturity index [5] but it needs a destructive test with high cost and inconvenience. It cannot be monitored on the same fruit continuously to investigate how environmental and fertilization parameters affect the ripeness at specific time points. Instead, farmers usually estimate the fruits' ripeness simply by skin color or firmness. However, skin color could be an unreliable or misleading indicator of fruit ripeness since late-season skin darkening can occur prior to harvest. Some fruits seem to be fully matured, judging by color, even though they are not soft. On the other hand, to prevent rot, low-temperature storage can produce fruits with reduced skin darkening [6]. Furthermore, color can confuse consumers as a fruit ripeness indicator by aesthetics, especially for organic fruits and vegetables. Estimating ripeness by firmness does not apply to some fruits, such as apples or watermelons. Some fruits' ripeness may be related to firmness, such as avocados, but squeezing them will potentially damage the fruits or further raise hygiene concerns. These issues mentioned are particularly important for organic agriculture because organic fruits often do not have identical appearances [7]. Measuring water content directly provides a quantitative method to assess fruit ripeness more precisely. In addition, the fresh fruit postharvest sector is dynamic with large and increasing consumer demands [8]. Monitoring the water content of fruits is a critical factor during postharvest [9]. If fruits are not appropriately stored, significantly decreased water content will occur and affect their taste and texture. Thus, it is vital to monitor continuously or discretely at chosen time points the water contents of fruits during the complete processes from preripe and ripe stages to storage periods before consumption, which can help to make informed decisions about fruit quality, production, and storage under varying environmental conditions.

Currently, the quantification of water content in fruits can be conducted in various ways [10], [11], including the oven-drying method [12] and the Karl Fischer titration method [13]. The oven-drying method requires subjecting fruit slices to drying within an oven until all moisture dissipates, followed by computation of the water loss percentage. The heating can change the tissue textures and alter their precise weights. In contrast, the Karl Fisher titration method offers a more precise methodology by employing specialized equipment for directly measuring water content using coulometric or volumetric titration to determine

Manuscript received 17 October 2023; revised 27 January 2024 and 2 May 2024; accepted 31 May 2024. Date of publication 4 June 2024; date of current version 21 June 2024. This work was supported in part by the NSF under Grant ENG-CMMI-1929953 and in part by the Mary and Richard Templeton endowment. Recommended by Lead Guest Editor Pai-Yen Chen and Guest Editor Chung-Tse Michael Wu. *(Corresponding author: Sen Bing.)*

The authors are with the Department of Electrical and Computer Engineering, Southern Methodist University, Dallas, TX 75205 USA (e-mail: sbing@smu.edu; kchawang@smu.edu; jchiao@smu.edu).

Digital Object Identifier 10.1109/JSAS.2024.3409229

water in samples [14]. Both approaches are destructive, demanding cutting or slicing of the fruit into samples that are difficult for real-time monitoring in farms or supermarkets. A low-cost, nondestructive, and convenient method for water content sensing is needed.

Utilizing nondestructive means to assess water contents in fruits has been a challenging need. X-ray and magnetic resonant imaging (MRI) have been used in laboratories to examine fruits, including apples [15], [16], [17], [18], [19], [20]. Particularly, the applications are to find watercore [21], a physiological disorder in which apples contain too much water in their intercellular spaces. Watercore affects the textures, firmness, and taste of apples significantly. During storage, apples with watercore develop alcoholic flavors and smells. They often also suffer from core browning or breakdown due to the excessive water [22]. Watercore is difficult to identify from fruits' appearance or by squeezing them. The reasons for watercore development are not well understood. Currently, farmers have to predict an optimum harvest time to avoid watercore by estimating their maturity, which is very difficult due to global climate changes. Tree pruning, thinning, and fertilization with correct ratios of calcium, boron, and nitrogen are believed to play important roles in reducing watercore risks [23], [24], [25]. However, the experiments have a long timeline and require a method to monitor water contents of apples as they grow. Thus, researchers wish to use nondestructive methods to investigate the development stages and reasons of watercore. However, it is clear that both X-ray and MRI are bulky, heavy, and expensive, preventing them from being used in an orchard to continuously monitor the water content of fruits. The fruits need to be picked to be examined, losing the opportunity for time-lapsed observation under different growth conditions. The study could not be done on a large scale either.

Radio-frequency (RF) electromagnetic waves may provide a nondestructive evaluation of fruits' status because of the high susceptibility to dielectric property changes caused by water content variations [26]. The interactions of electromagnetic fields within fruit tissues at different water percentages affect wave scattering and provide noninvasive and high-sensitivity sensing. The dielectric property can be evaluated by resonant frequency shifts and magnitude changes of reflection coefficients in wave propagation measurements. Recent RF devices and integrated circuits are cost-effective to manufacture Internet-of-Things (IoT) sensing devices, in which low-power electronics include short-distance data communication, sensor drivers, and memory, for large-scale implementation. Their sizes are also small and suitable to be integrated into wearables for fruits.

Microwave resonators typically have smaller footprints [27] compared with waveguides, which is beneficial considering the small size of fruit. Utilizing dielectric or cavity resonators [28], [29], [30] for such sensing applications presents practical issues. The rigid configurations of these types of resonators are not suitable for curved surfaces of fruits/vegetables. Planar circuits or antenna resonators are more appropriate, and recent advances in circuit and antenna fabrication on flexible substrates make them easy to be attached and conformed to the fruit skin. However, poor resonance at microwave frequencies in planar loop resonators fails to provide reliable and sufficiently deep penetration of fields into tissues due to the impedance matching issue [31]. Using a dynamic matching circuit to achieve a high-quality factor is possible but makes it bulky with design constraints. The technical challenge in such a conformal microwave resonator is to achieve a high-quality factor without sacrificing the features of being planar with a small form factor.

Split ring resonators have been used in planar circuits and provide good resonance for sensing [32], [33], [34], [35]. However, they require energy coupling from the outer ring to the inner ring, which provides the resonance of interest. The coupling induces more insertion losses. The two rings inevitably bring multiple harmonics that can reduce the quality factor of the desired resonance. Both rings are susceptible to environmental changes, bringing more interference concerns for a wearable in which one side of the device is facing the free space. Their spectral shapes of harmonics vary differently from the variations of effective permittivities. Kilpijärvi et al. [36] designed a reflection-based sensor for human hydration sensing using a complementary split-ring resonator (CSRR) pattern, fabricated on an SubMiniature version A (SMA) connector connected to a vector network analyzer (VNA). The SMA connector served as a feeding structure for the CSRR. However, CSRRs have higher insertion losses as the inner split ring, creating the required resonance, is indirectly excited by the current in the outer ring. This effect reduces field penetration depth into the tissues.

With the intention to keep the resonator device architecture simple, our preliminary work [37] developed a self-tuned method for impedance matching in a planar loop resonator by embedding a concentric metal pad. The principle is based on the presence of a center pad to provide additional distributed capacitances from the gap between the loop and metal pad [38] and additional mutual inductance [39] between metal strips across the gap owing to coupled magnetic fields. The spacing between the loop and center pad tunes the distributed reactance to match the port impedance in the desired frequency range. The resonance becomes significantly improved without changing the overall size of the loop. The loop resonators have been made into compact and flexible forms with high resonance performance for near-field sensing. Applications have been investigated for human hydration monitoring [40], [41], [42]; subcutaneous implant localization [43], breast cancer detection or imaging [44], [45]; and skin cancer distinction [46]. The high-quality factor also enhanced transcutaneous wireless power transfer [47]. Utilizing a similar tuned loop resonator, this work aimed to develop an efficient, low-cost, and flexible sensor that can be attached to the fruit surface to estimate and monitor its water content. To enhance fruit sensing capabilities, the configuration has been redesigned and optimized to operate at 1.42 GHz, as opposed to the 900 MHz frequency used for human hydration monitoring [40]. This adjustment also involves a more compact footprint, ensuring a better fit for the fruit-sensing application. Apple is targeted in this work to demonstrate the concept for its high volume in the market [48] and convenience in experiment operations.

II. Sensor Design

Considering the curvature of the fruit surface, a flexible polyimide film (DuPont™ Pyralux FR9220R, Wilmington, Delaware) was chosen for resonator fabrication. Sufficient flexibility could provide firm contact onto the fruit skin. The thickness of the film was chosen to be 76 μm. It had a dielectric

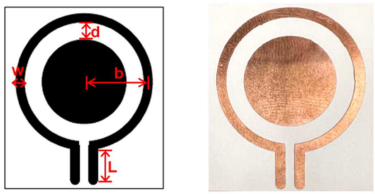

Fig. 1. (a) Configuration of the sensor with radius $b = 11$ mm; the loop width $w = 2a = 1.6$ mm; the tuning gap $d = 2.9$ mm between the pad and loop. (b) Photograph of the sensor.

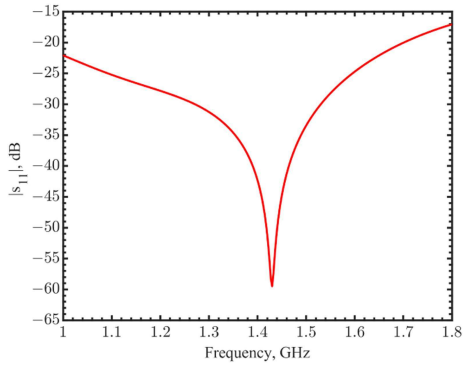

Fig. 2. Reflection coefficients in simulation.

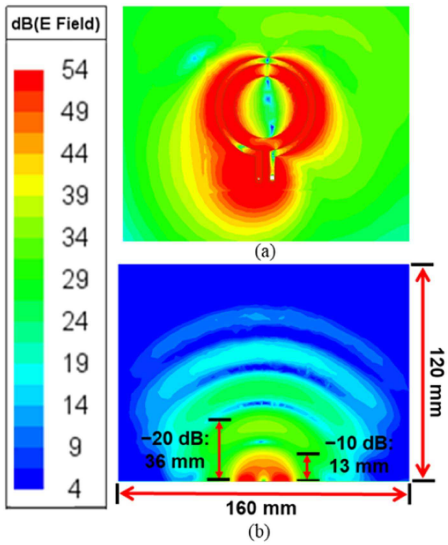

Fig. 3. Cross sections of electric field distributions from the tuned loop resonator. (a) Top view and (b) side view into the apple tissue.

constant of 3.2 with a loss tangent of 0.022. The film had a layer of 70-μm thick copper. In simulations, these parameters were the same as the ones in fabrication. The sensor consisted of a loop as the resonating element and a metal pad as the tuning element, as shown in Fig. 1(a). The driving voltage is applied to the loop gap, generating oscillating currents along the loop. Resonance occurs when the wavelength of the traveling current roughly matches with the loop's circumference. Storer [49] found the loop length is not exactly but close to the integer numbers of the half resonance wavelengths. At resonance, the current freely circulates in the loop, forming a standing wave. The reflected power from the loop toward the power source through the gap becomes minimum. In this case, the imaginary part of the impedance becomes almost zero, making the loop impedance resistive, which is essentially the radiation resistance of the loop. Away from resonant frequencies, reactances due to the phase differences between voltages and currents make the resonator act like an *R-L-C* in series resonator. Each harmonic order of resonance can be modeled as an *R-L-C* branch. The *RLC* pairs in parallel [37] determine the overall impedances at different frequencies. Within the frequency range of interest, the resonator equivalent circuit can be used to decide the system reflection coefficient and spectral shapes.

The copper pattern was etched after photolithography was applied with a photomask on the photoresist-covered film. A photo of the resonator is shown in Fig. 1(b). The radius of the loop resonator b was 11 mm with a connecting stub length $L = 6$ mm, which was prepared for a connector to the measurement port. The incident power through the port is -5 dBm, both in the simulations and the following measurements. The metal width w was 1.6 mm. The gap between the loop and the center pad d was chosen to be 2.9 mm, which tuned the resonance below -59.48 dB, as shown in Fig. 2. In this simulation, the apple tissue with a dielectric constant of 29 and a conductivity of 0.81 S/m was chosen to fit with the measured spectral curve. The resonance provided a confined and sufficiently deep field distribution into the apple tissue. Fig. 3(a) shows strong fields across the gap and around the loop. The -10-dB and -20-dB attenuation depths from the loop surface in Fig. 3(b) were 13 mm and 36 mm, ensuring sensing of the effective permittivity deep inside the fruit tissue. Without tuning, the resonance reached only -24.29 dB in simulations. Fig. 4 compares the internal electric fields produced by the tuned and untuned loops which are placed on the apple surface skin. The fields are shown at the depths of 5, 15, and 30 mm inside the apple. Comparing the field penetration depths in Fig. 4(a) and Fig. 4(e), which show the vertical cross-sectional views, the -10 dB depths were 11 mm and 5 mm for tuned and untuned loops, respectively. Fig. 4(b)–(d) and (f)–(h) shows the field distributions at specific depths in the horizontal cross sections parallel to the surface skin. Comparing the same depths, the field strengths decay much faster for the untuned loop. At the 15-mm depth, the highest field magnitudes in the center have a difference of 1.62 dB between these two loops. At the depth of 30 mm, the field magnitude difference between the two loops at the highest points was 3.39 dB. These show that stronger electrical fields within the tissues have a better resonance for the tuned loop, by which a larger volume of dielectric properties inside the apple are included in the effective permittivity experienced by the sensor.

III. Water Content Experiments

A. Measurement Setup

To validate the concept of continuous monitoring, long-term dehydration experiments of apples were conducted to continuously record the reflection coefficients when apples lost water from fresh to relatively dehydrated. Resonant frequencies were

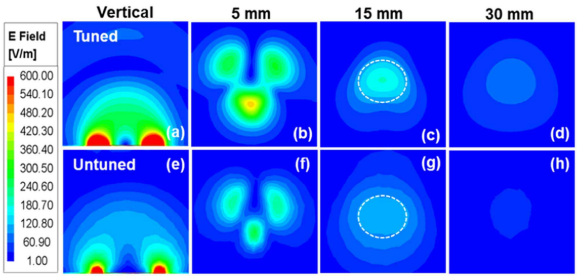

Fig. 4. Comparison of electric fields. (a) Vertical cross section into the apple from the tuned loop at the bottom, and (b)–(d) horizontal cross sections of the apple at depths of 5, 15, and 30 mm from the tuned loop on the surface skin. (e) Vertical cross section inside the apple with an untuned loop at the bottom, and (f)–(h) horizontal cross sections of the apple at depths of 5, 15, and 30 mm from the untuned loop on the surface skin.

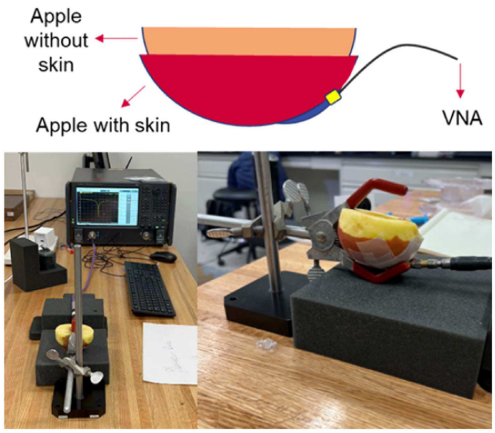

Fig. 5. Setup of measurements.

extracted from reflection coefficients. Fig. 5 shows the experiment setup. The sensor was applied and conformed onto the apple and connected to a VNA (Keysight PNA N5227B). A medical-grade tape (3 M Nexcare Durapore Durable Cloth Tape, USA) was used to attach the sensor to the apple to ensure stable and firm contact. The apples chosen were Fuji apples from a local supermarket with similar sizes and shapes. As the purpose is to develop a nondestructive sensor, the apple skin around the area where the sensor contacted it was preserved. To speed up water evaporation, the skin away from the sensor was shaved, and part of the internal tissues were exposed to air during the experiment. The thickness of the apple under the experiment was around 50 mm. The cut plane was above the core. Air circulation was applied to accelerate water evaporation in the apples. Due to the high sensitivity of the tuned sensor, mechanical tension variations from weight changes to the coaxial cable induced small movements between the apple and cable, which caused measurement fluctuations. To improve stability, a laboratory positioning system (Parker Daedal Division, PA) with a clamp (Fisher™ Castaloy™) was used to stabilize the subject. In addition, considering the significant weight loss during the long-term experiments, porous styrofoam was placed underneath the clamp to support the measurement subject and alleviate cable tension.

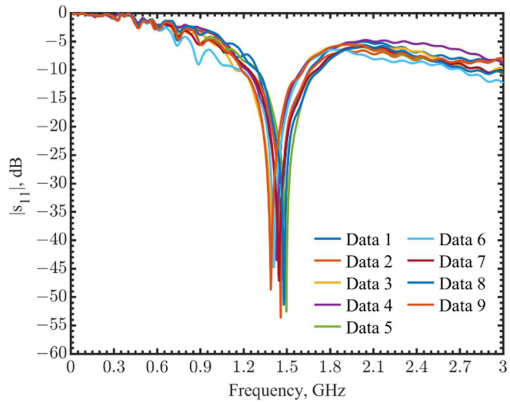

Fig. 6. Comparison of measured reflection coefficients in nine Fuji apples.

A digital scale recorded the weight of the apple every minute during the experiment to monitor water loss.

The presence of mold in fruits initiating biological degradation of tissues could alter the fruit's physical and chemical composition and potentially affect its dielectric properties. Dry air circulation is used to ensure no mold growth and visual inspection confirms it. Nine fresh apples free of mold were tested for the measurement setup's stability and repeatability. Fig. 6 compares reflection coefficients from 0.1 to 3 GHz for these nine apples. Similar spectral curves with sharp resonance overlapped, indicating that the setup was reliable. Although the nine apples had similar sizes and shapes, the resonant frequencies ranged between 1.388 and 1.496 GHz. This variation was likely due to the curvature and water content distribution within individual apples. The quality factors, calculated from $Q = f_0/\Delta f_{3\,\mathrm{dB}}$ where f_0 is the resonant frequency and $\Delta f_{3\,\mathrm{dB}}$ is the 3-dB bandwidth, were around 120. The sharp resonance remained reliable to ensure measurement sensitivity.

B. Continuous Long-Term Monitoring

Reflection coefficients across 0.1−3 GHz were automatically recorded every minute for 38 h. The experiments were conducted at room temperature to avoid apple tissue damage from the heat that may occur using an oven. A program in MATLAB automatically sorted out resonance points in the frequency range of 0.1−3 GHz. The experiments were repeated with four apples under the same protocol. Fig. 7 shows the measured resonant frequencies during the 38-h experiments. All four datasets show continuously and monotonically increasing trends of resonant frequencies during water evaporation. The averaged start and end reflection coefficients among these four long-term experiments are compared in Fig. 8(a). The error bars indicate standard deviations. The beginning resonant frequencies were 1.460, 1.457, 1.394, and 1.430 GHz, whereas the end resonant frequencies were 1.974, 1.956, 1.870, and 1.879 GHz, respectively, as shown in Fig. 8(b). To compare the effective permittivities of apples during the long-term experiments, simulations were conducted. The real and imaginary parts of permittivities were fitted in simulations to match the measured spectral curves at the selected time points when the weight loss percentages

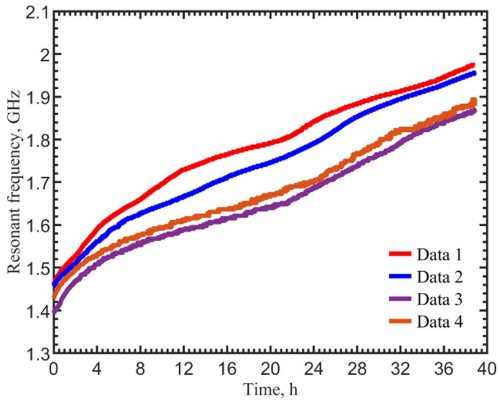

Fig. 7. Comparison of resonant frequencies in time during the continuous long-term water content monitoring measurements.

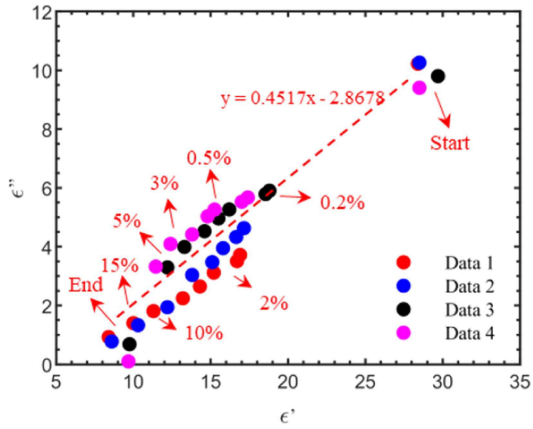

Fig. 9. Permittivity comparison for different weight loss in the four 38-h experiments.

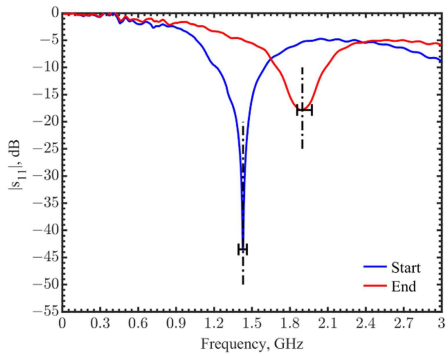

(a)

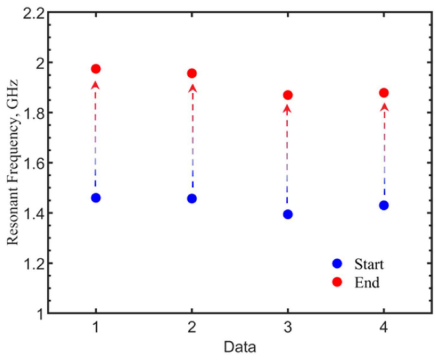

(b)

Fig. 8. Comparison of the start and end measurements in four long-term monitoring experiments. (a) Spectral curves with averaged start and end frequencies. The error bars are their standard deviations. (b) Individual resonant frequency changes.

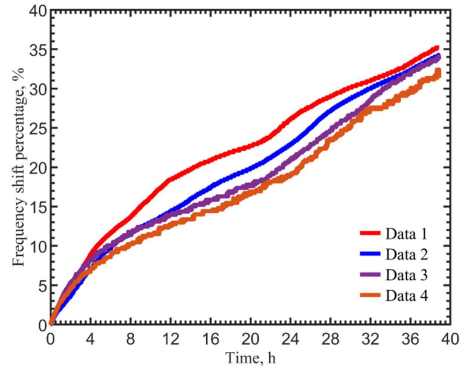

Fig. 10. Comparison of resonant frequency shift percentages over time during the continuous long-term measurements.

were 0.2%, 0.5%, 2%, 3%, 5%, 10%, and 15%, as well as at the start and end points of experiments. Fig. 9 shows the permittivities comparison for the four apples. A trendline was added to estimate the relationship between the real and imaginary parts of permittivities during dehydration. For fresh apples, the average real and imaginary parts of complex permittivities were 28.775 and 9.926. At 1.435 GHz, the average conductivity calculated from the imaginary permittivity was 0.792 S/m. After dehydration, the average real and imaginary parts of permittivities and conductivity were 9.108, 0.619, and 0.067 S/m. The permittivities changed more significantly at the beginning of the experiments. When the initial 0.2% water weight was lost, the changes in average real and imaginary parts of the permittivity were 11.213 and 5.605. When another 0.3% of water was lost, the changes were 0.335 and 0.088. This might be due to the evaporation process from the shaved surface. As the water evaporated from the shaved surface, the fields immediately experienced a significant change in effective permittivity due to the dried area at the top. Then, the water inside the apple started to diffuse and rise from the bottom to the shaved surface area by osmosis. The water concentration did not change significantly below the dried area. The effective permittivity changes were slower in time as the water concentrations redistributed over a large volume more evenly. The abrupt change of resonant frequencies from 1.435 to 1.446 GHz when 0.2% water was evaporated validated that the electric fields penetrated sufficiently deep beyond the core, judging from the dried area, and the sensor should be able to detect the water content of the whole apple.

For normalized comparison, the resonant frequency at the beginning of the experiment was used as the baseline, and frequency shifts in percentage were calculated at other time points. Fig. 10 shows the measured resonant frequency shift

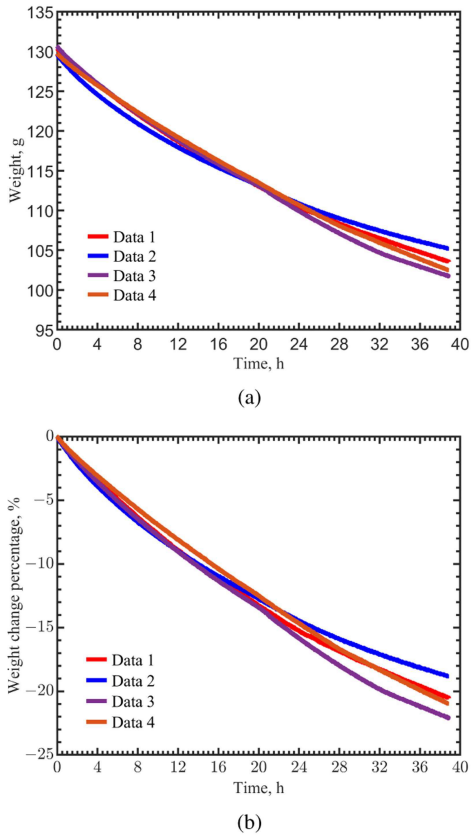

Fig. 11. Weight changes during the long-term monitoring experiments. (a) Actual weight in grams. (b) Weight change percentages.

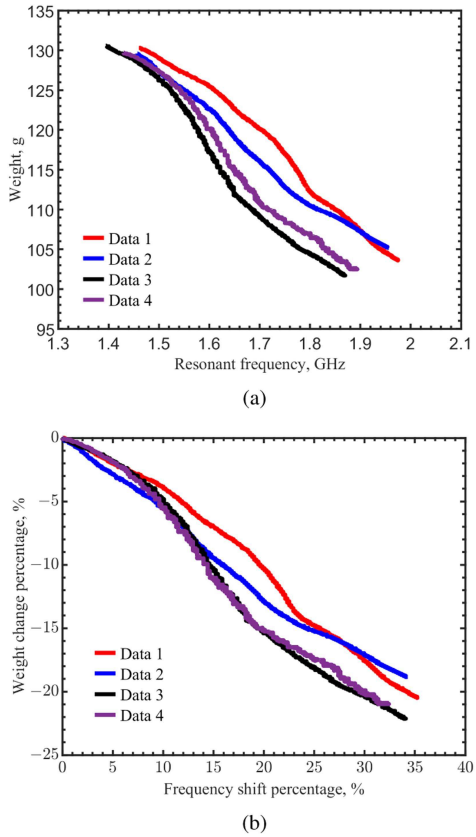

Fig. 12. Comparison of four apples during the long-term experiments. (a) Weight as a function of resonant frequency. (b) Weight change percentage as a function of resonant frequency shift percentage.

percentages over time among these four experiments. They have similar trends with the end frequency shifts of 35.2%, 34.3%, 34.1%, and 31.4%. Fig. 11(a) shows the weights recorded over time. The apples were prepared with similar weights of 130.3, 129.6, 130.6, and 129.7 g at the beginning. After 38 h of evaporation, the end weights became 103.5, 105.2, 101.7 and 102.5 g, respectively. Similarly, using the weight at the beginning as the baseline, weight loss percentages are shown in Fig. 12. The respective weight loss percentages were −20.57%, −18.83%, −22.13%, and −20.97% after 38 h. Fig. 12(a) shows the apple weight as a function of resonant frequency. As both the resonant frequency and weight change over time appear to be repeatable with some degree of linearity, it suggests a predictable relationship between the resonant frequency and apple water content change, which is the main reason for weight loss. The weight change percentage as a function of the frequency shift percentage is compared in Fig. 12(b). All four datasets showed continuously and monotonically decreasing trends from the baseline while water evaporated. The relationship indicates the resonant frequency and water content are highly correlated.

However, there were discrepancies among these four curves. Apples with the same weight losses yet had slightly different end resonant frequencies. It could be explained by the effects of apple shapes and inhomogeneous water evaporation from the skin-shaved portions. Water loss began first from the shaved part. Water inside needed to diffuse gradually from deeper parts of apple tissues to the exposed surface. This procedure was slow

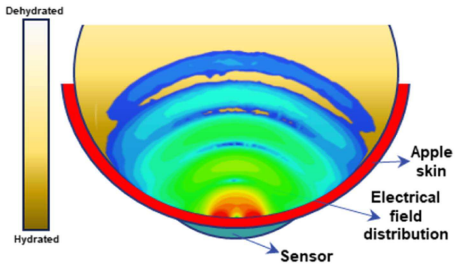

Fig. 13. Cross-section view of electric field distributions compared with the water content distributions after water gradually evaporated after 38 h from the top surface where the skin was shaved.

at room temperature because osmosis purely depended on water balances across cell membranes. As the water left the surface, more distances were needed for water to travel across multiple cell membranes or in the extracellular spaces to the top surface of the tissues to be evaporated. The area of the apple with skin covered was still fresh after 40 h of evaporation, whereas the part exposed to air had completely become dry with colors changed. The apples, through such inhomogeneous evaporation, would have nonuniform water distributions along the tissue depths, as illustrated in Fig. 13. The electrical field distributions from a simulation were overlapped on the gradient illustration of water distributions. The bottom area where the sensor produced

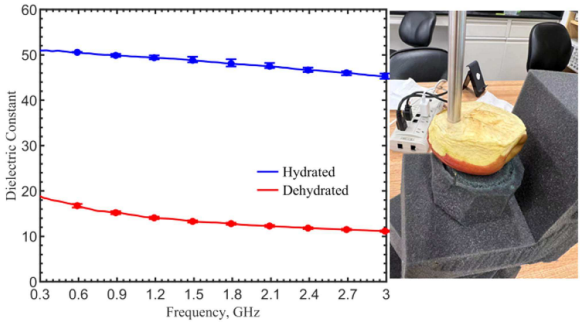

Fig. 14. Comparison of dielectric constants measured with a coaxial probe on the hydrated layer (blue) and dehydrated layer (red) of an apple.

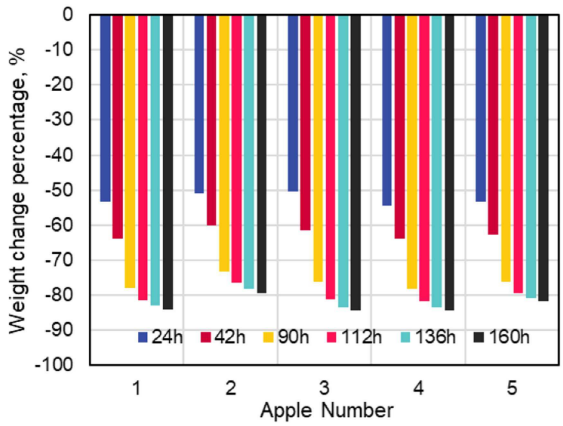

Fig. 15. Weight changes of five apples during the dehydration process.

higher field densities had more water contained because the water had to diffuse a much longer distance to the top surface where water evaporated. The effective permittivity experienced by the resonator was dominated by the volume near the sensor. With the tuned resonance, deeper field penetration into the apple covered a larger volume that affected the effective permittivity. As the fields could reach into more dehydrated areas in the apple, the effective real part of the permittivity was lower because the fields interacted with less water, leading to a higher resonant frequency. The inhomogeneous water evaporation and diffusion thus created discrepancies at the end of long-term experiments with larger frequency differences compared with the ones in the beginning, as shown in Fig. 7. To verify this assumption of inhomogeneous effects, dielectric properties measurements were conducted on an apple using a coaxial probe kit (Keysight N1501 A). The apple was held in the same setup as the one in Fig. 5 with water evaporation from the skin-shaved surface. Measurements were conducted at two areas on the same apple. One was on the shaved part, where dehydrated tissues had been exposed to air for 41 h. The other area had skin covered during water evaporation but had its skin shaved right before the probe measurements. The measured dielectric constants are shown in Fig. 14. Each dataset with error bars was obtained from three locations in the same areas. The averaged values showed the dielectric constants had a slight dependence on frequency within the 1.4−1.9 GHz range, and the hydrated and dehydrated tissues had large differences in dielectric constants. It was noted that pressure on the apple tissues affected the measurement results. Because the shaved apple surface was not perfectly flat, the probe was pushed into the tissues with some pressure to make a solid and stable contact. It could be seen that the probe left a circle mark after measurements. It was noticed that a little water was squeezed out from the apple tissues and accumulated around the probe head. The water inevitably increased the measured dielectric constants. They were higher than the effective permittivities used in simulations that were obtained from fitting the spectral curves of the reflection coefficients by our sensor that did not need to apply pressure on the apple surface to obtain reliable measurements.

The high contrast of the dielectric constants verified the assumption about inhomogeneous water evaporation in apples. The measurements also showed the fields from the tuned resonator could radiate sufficiently into the apple to detect the water loss in deeper depths. To be noted that the partially shaved apples in the experiments were for the purpose of accelerating water evaporation in order to create different water contents. In actual applications, the measured apples would not have such a condition. Thus, the discrepancy caused by inhomogeneous evaporation may probably not be an issue. However, if the water distributions inside an apple are not uniform, perhaps due to its shape, growth conditions, such as uneven sun exposure, insect bites, mechanical damages, or infection that causes watercore [17], [21], [22], the resonant frequencies on different locations of an apple may show discrepancies. In such a case, either an average value should be taken, or the specific apples should be treated as anomalies for studies. A detailed investigation of watercore detection will be discussed in a later section.

C. Total Water Content

The total water content could be assessed by extending the dehydration experiments until the apples were completely dried out. Thus, the total water content could be related to the initial resonant frequency. However, the natural water evaporation process to completely dry out an apple could take several days or weeks, and apples become rotten, affecting tissue structures. In addition, the apple curvature and its skin also significantly changed, creating air gaps between the attached sensor and its skin. Thus, it is impractical to simply extend the experiment time.

An experiment was designed specifically to investigate the correlation between resonant frequency and total water content. Cooling fans were used to accelerate water evaporation at a constant room temperature to avoid tissue, surface curvature, or skin changes from heat. The air circulation also avoided the risks of rotting. Five fresh Fuji apples with similar shapes were measured at 0.1−3 GHz and weighed. Each apple was then cut into five pieces, including four slides and the core. The cut pieces were organized and labeled into five groups. They were placed within the air-circulating space with the intention of equal water evaporation among all groups. Each group was weighted together and measured at six time points of 24, 42, 90, 112, 136, and 160 h. Fig. 15 shows the weight change percentages of the five apples during dehydration. After 112 h, the weight losses became slow, and the weights remained constant after 160

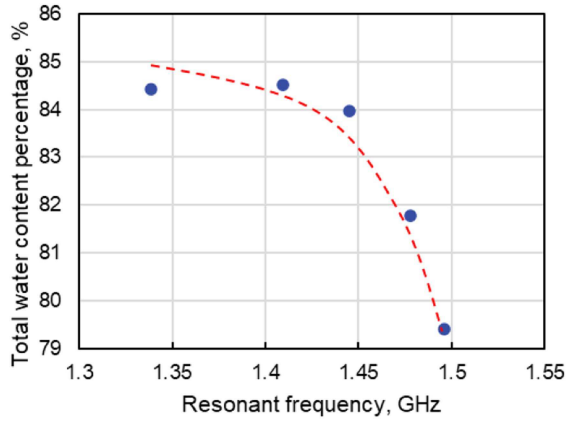

Fig. 16. Total water content percentage as a function of measured resonant frequency.

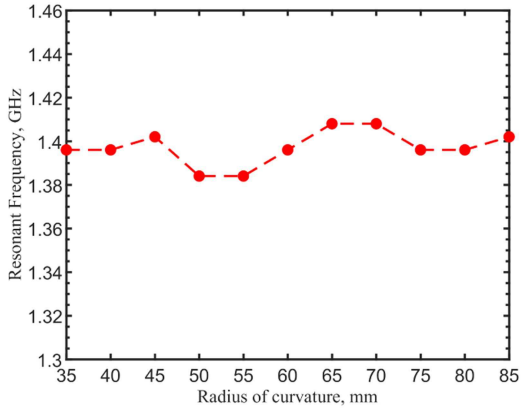

Fig. 17. Resonant frequency as a function of curvature radius.

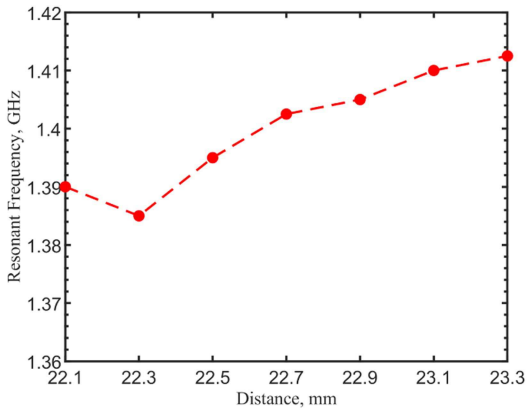

Fig. 18. Resonant frequency as a function of distance between the apple core and the sensor on its skin.

h, which was assumed that the apples were fully dehydrated. The total water content percentages for these five apples were measured as 83.97%, 79.41%, 84.44%, 84.51%, and 81.79%, roughly within the same range studied in the literature [1], [2]. The corresponding measured resonant frequencies prior to the cutting and dehydration were 1.445, 1.496, 1.338, 1.409, and 1.478 GHz, respectively. Fig. 16 shows the total water content percentage as a function of resonant frequency. The result matched with the expectation that a higher water content leads to a lower resonant frequency because of its higher effective permittivity

IV. Discussion

A. Physical Shapes

The physical shape and structure of each apple can potentially affect the resonant frequency, such as the surface curvatures or its core size. The sensor was designed and fabricated on a flexible polyimide substrate to conform to the apple skin. Curvature apples affect the field distributions within the apple, varying its resonance. Simulations were conducted with different apple curvature radii in a range of 35−85 mm, mimicking their potential growth stages. Fig. 17 shows the resonant frequencies in the selected curvature radius range. The resonant frequency variation is limited to the range of 1.384−1.408 GHz, indicating the resonator could be reliably used in different apple shapes but may need calibrations for sizes.

Apple core has less water content and significantly different dielectric properties from the main tissue. Inside the core, the seeds surrounded by air decrease the effective permittivity compared with the moist apple tissues. During the apple water content experiments in Section III, different measured locations or apple core sizes would vary the equivalent distance between the sensor and the core, affecting the effective permittivity experienced by the fields within the sensing volume. To investigate the effect, simulations were carried out by placing an apple core at different depths with respect to the sensor on the skin. The apple core diameter was selected as 18.59 mm, which was an average value according to [50], with a distance range of 22.1−23.3 mm to the skin. Because of the deeper field penetration of the tuned resonator, it was expected that the core location would affect the resonant frequency. Fig. 18 shows the resonant frequency as a function of the distance between the core and the surface. There was a 22.5 MHz shift when the distance changed from 22.1 to 23.3 mm.

Although both curvatures and core locations lead to limited resonant frequency shifts of 25 and 22.5 MHz, the combined effects could explain the resonant frequency discrepancies at the beginning of the long-term experiments in Fig. 7. Because of the high sensitivity of the tuned resonance, such effects need to be considered in practical scenarios.

B. Watercore Detection

Watercore is an internal disorder for apples in which the intercellular spaces are filled with excessive fluid, leading to characteristic translucent tissues [51]. It generally happens around the vascular bundles [52] and shows as a water-soaked area [53]. Watercore is typically found when apples mature in extreme temperatures [54], which in turn advance their maturation periods, as temperature is one of the key factors affecting apple ripening [55]. High temperature accelerates maturity because

of the increased respiration rate, enzyme reaction, and starch-to-sugar conversion in apples. On the other hand, Marlow and Loescher [51] and Willams and Billingsley [56] reported that cold temperatures could also affect watercore forming, which is related to sorbitol metabolism. Farmers with the intention of speeding up apple's ripeness specifically meet watercore cases often. Mildly affected apples were appreciated and sold at premium prices in some regions due to their sweetness [17], [25]. However, severe watercore can induce browning [52] and alcoholic flavors [17] in apples, diminishing their values [22]. Apple watercore occurrence can be high and varies dramatically by region and season due to different climates. Tomana and Yamada [57] reported that the quality and sugar contents of Fuji apples grown in Japan were affected greatly by local temperatures. Zhang et al. [58] reported a study that 52% of purchased Fuji apples in local fruit markets under U.S. Department of Agriculture instructions were identified as watercore samples. Han et al. [59] reported that in two batches of apple samples collected at a domestic orchard in China, the mean watercore severity indexes were 6.11% and 10.2%, whereas the maximum index values in individual batches reached 18.04% and 34.87% [60]. It is considered severe when the watercore severity index is higher than 10%.

It is challenging to visually inspect watercore in apples because it has no clear external features [60]. The cross-section view can show the watercore after cutting apples, which is destructive and costly. Several nondestructive methods for apple watercore detection have been reported, such as thermal imaging with infrared signals [61], MRI [19], X-ray computed tomography [17], and near-infrared hyperspectral imaging [62]. However, these technologies cannot satisfy the demand for mass samples in industry due to the high costs and being time-consuming [31]. Our tuned sensor can be used for nondestructive detection of watercore due to its sensitivity to the effective permittivity change from watercore. The water-filled area brings much higher water content than a normal apple, resulting in a higher effective permittivity [63]. Apples with known watercore were difficult to find in markets for experiments, thus simulations were conducted to investigate the feasibility.

In the simulations, a layer of water was added to the apple models to mimic the watercore. Since watercore typically starts from vascular bundles and gradually spreads to the whole apple, the water layer depth was selected at 22.5 mm, the average distance between the apple core edge to its skin [50]. According to severity, watercore can be classified into three levels: light, medium, and strong, with the related damaged tissue proportion as 17.4%, 47.14%, and 74.53%, respectively [19]. To mimic the watercore in different levels, water layer thickness varied from 1 to 22 mm in simulations. Fig. 19(a) compares the spectral curves at the selected thickness, whereas Fig. 19(b) shows the related resonant frequencies. A 50-MHz frequency shift could be observed with only 1 mm of the water layer thickness. Also, the reflection coefficient magnitude changed to −37.3 dB from −59.5 dB. Resonant frequency continued shifting to 1.14 GHz as the water layer thickness increased to 22 mm, representing the strong watercore level. A 290-MHz frequency shift covered the range from a healthy apple to one with a severe watercore. A wide frequency range and significant change of the quality

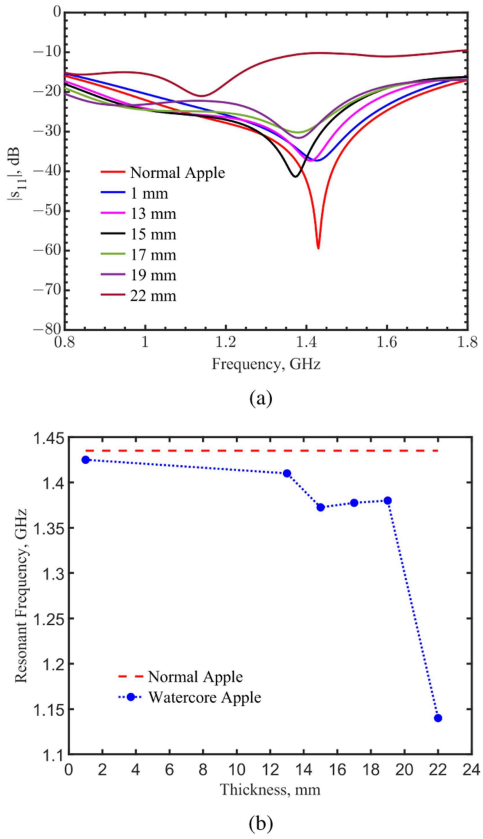

Fig. 19. Comparison of different watercore levels. (a) Spectral shapes and reflection coefficients with different watercore thicknesses. (b) Resonant frequency as a function of watercore thickness.

factor, judging from the spectral shapes, indicated the high sensitivity of the tuned sensor for the feasibility of detecting watercore.

C. Additional Application for Vegetables

The tuned flexible sensor could also be used to monitor and estimate the water content of vegetables. Potato is selected to demonstrate the concept because it is one of the most significant vegetable crops globally [64]. Potatoes are widely consumed as processed into French fries and chips. The massive market of fried potato chips will reach $33.3 billion globally in 2023 [65]. Although the global production level has increased by 20% since 1990, about 32% of potatoes were lost yearly due to the lack of proper management, storage, or processing [64], [66]. Water content is one of the most important parameters affecting the quality of the product during the drying and frying in potato processing [67]. For example, knowing water content can adjust the temperatures of ovens and fryers to produce uniform drying in potato chip processing, providing better taste. Often, the potatoes grown even in the same batch, location, or farm do not have the same water contents. Frying with a controlled temperature specific for a certain moisture level can ensure crispiness without burn marks [68], [69], [70]. The taste and quality of deep-frying potato chips for different potato cultivars with various moistures can be optimized with controlled temperatures and timing if the initial water contents are known [71], [72], [73]. Proper storage

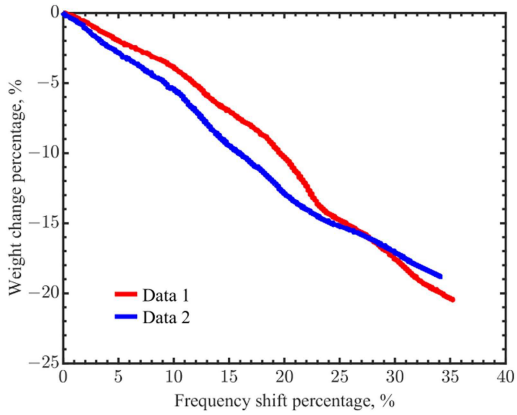

Fig. 20. Comparison of weight change percentage as a function of resonant frequency shift percentage for two potatoes during the long-term monitoring experiments.

will preserve the potatoes' freshness, preventing spoilage or shrinkage due to significant water loss [74], [75]. Thus, knowing the water content of potatoes in real-time and in situ can help make informed decisions.

Similar to the apple water content assessments, water measurements in potatoes commonly utilize oven-drying or freeze-drying methods [76], which are destructive. Based on the same protocol, continuous long-term experiments in Section III were repeated for potatoes to investigate the feasibility of nondestructive sensing. The sensor was attached to the potato skin in a similar way to apples. The sensor locations on two different potatoes were chosen to be the middle point as the potato was laid flat with its longer dimension horizontally. The middle point provided a relatively flat area without eyes or root scabs. One third of the skin on the top of the potato was shaved to accelerate water evaporation in an air-circulation space. Reflection coefficients were recorded at each minute by the VNA for 20 h. The initial resonant frequency was used as the baseline, and frequency shifts in percentage were calculated at later time points. The weights of the potatoes were recorded at the same rate by an electronic scale. The weight change percentages were calculated with the initial weight as the baseline. Similar to Fig. 12, the weight loss percentage as a function of resonant frequency shift percentage is shown in Fig. 20. The curves indicated a stable relationship between the water content loss and resonant frequency, validating the feasibility of sensing water content in potatoes.

V. Conclusion

In this work, we demonstrated a tuned planar flexible microwave resonator that can conform to the fruit skin to measure and continuously monitor the water content nondestructively. The resonant frequency of the sensor is susceptible to dielectric property changes due to water content variations. The high-quality factor resonance in the tuned loop provides wider and deeper electromagnetic field distributions into the fruit tissues, ensuring a high sensitivity to water changes. Apples are chosen for the demonstration of feasibility. Measurements and simulations were conducted to validate the feasibility of noninvasive sensing. Multiple experiments, including continuous long-term water content monitoring and total water content assessment, have been conducted to validate the principle. Discrepancies among measurements are investigated. The effects from inhomogeneous water evaporation in experiments, apple surface curvatures, and core locations are shown to contribute to the measurement fluctuations. Multiple measurements on apples show distinct and repeatable trends of resonant frequency shifting from hydrated to dehydrated states. Watercore detection was investigated and verified by a series of simulations. The demonstrations with potatoes additionally show the feasibility of water-sensing applications of vegetables. With the advantages of being planar, low-cost, flexible, highly sensitive, and the capability to be integrated with IoT electronics, the nondestructive water-content sensors show great potential for applications in the agriculture and food industry.

Since this work is in the stage of concept validation, we temporarily rely on a VNA to power the sensor and collect the data, ensuring that we can validate the sensing concept with needed high accuracy and reliability. Moving forward, the complete product will operate independently with active elements such as microprocessors and power management circuits to keep costs low. Alternatively, the sensor can be fabricated based on RFID technology, allowing for battery-free operation. In this configuration, a separate reader can organize and collect data from numerous sensors over large agricultural areas, supporting massive sensor deployment in extensive farming operations.

References

[1] B. M. Popkin, K. E. D'Anci, and I. H. Rosenberg, "Water, hydration, and health," *Nutr. Rev.*, vol. 68, no. 8, pp. 439–458, Aug. 2010.
[2] USDA, "Apples, raw, with skin (includes foods for USDA's food distribution program)," U. S. Department of Agriculture, Washington, D.C., USA, Tech. Rep., Apr. 1, 2019. [Online]. Available: https://fdc.nal.usda.gov/fdc-app.html#/food-details/171688/nutrients
[3] C. Frenkel and T. G. Hartman, "Decrease in fruit moisture content heralds and might launch the onset of ripening processes," *J. Food Sci.*, vol. 77, no. 10, pp. S365–S376, Oct. 2012.
[4] J. Ackermann, M. Fischer, and R. Amado, "Changes in sugars, acids, and amino acids during ripening and storage of apples (cv. glockenapfel)," *J. Agricultural Food Chem.*, vol. 40, no. 7, pp. 1131–1134, Jul. 1992.
[5] A. A. Kader, "Fruit maturity, ripening, and quality relationships," in *Proc. Int. Symp. Effect Pre- Postharvest Factors Fruit Storage*, 1997, pp. 203–208.
[6] P. J. Hofman, B. A. Stubbings, M. F. Adkins, R. J. Corcoran, A. White, and A. B. Woolf, "Low temperature conditioning before cold disinfestation improves 'HASS' avocado fruit quality," *Postharvest Biol. Technol.*, vol. 28, no. 1, pp. 123–133, Apr. 2003.
[7] Sigma Test & Research Centre, "Five ways to identify organic food," Sigma Test & Research Centre, New Delhi, India, Tech. Rep. [Online]. Available: https://www.sigmatest.org/blog/five-ways-to-identify-organic-food/
[8] G. P. Moreda, J. O.-Cañavate, F. J. G.-Ramos, and M. R.-Altisent, "Non-destructive technologies for fruit and vegetable size determination–A review," *J. Food Eng.*, vol. 92, no. 2, pp. 119–136, May 2009.
[9] P. Chen and Z. Sun, "A review of non-destructive methods for quality evaluation and sorting of agricultural products," *J. Agricultural Eng. Res.*, vol. 49, no. 2, pp. 85–98, 1991.
[10] S. Yazgan, A. Bernreuther, F. Ulberth, and H. D. Isengard, "Water-an important parameter for the preparation and proper use of certified reference materials," *Food Chem.*, vol. 96, no. 3, pp. 411–417, Jun. 2006.
[11] K. Huynh-Ba, *Handbook of Stability Testing in Pharmaceutical Development : Regulations, Methodologies, and Best Practices*, 1st ed. New York, NY, USA: Springer, 2009.

[12] A. Korpa and R. Trettin, "The influence of different drying methods on cement paste microstructures as reflected by gas adsorption: Comparison between freeze-drying (f-drying), d-drying, p-drying and oven-drying methods," *Cement Concrete Res.*, vol. 36, no. 4, pp. 634–649, Apr. 2006.
[13] E. Tavčar, E. Turk, and S. Kreft, "Simple modification of Karl-Fischer titration method for determination of water content in colored samples," *J. Anal. Methods Chem.*, vol. 2012, Jan. 2012, Art. no. 379724.
[14] K. Fischer, "Neues verfahren zur maßanalytischen bestimmung des wassergehaltes von flüssigkeiten und festen körpern," *Angewandte Chemie*, vol. 48, no. 26, pp. 394–396, Jun. 1935.
[15] S. Y. Wang, P. C. Wang, and M. Faust, "Non-destructive detection of watercore in apple with nuclear magnetic resonance imaging," *Scientia Horticulturae*, vol. 35, no. 3, pp. 227–234, 1988.
[16] C. J. Clark, J. S. MacFall, and R. L. Bieleski, "Loss of watercore from 'Fuji' apple observed by magnetic resonance imaging," *Scientia Horticulturae*, vol. 73, no. 4, pp. 213–227, Apr. 1998.
[17] E. Herremans et al., "Comparison of X-ray CT and MRI of watercore disorder of different apple cultivars," *Postharvest Biol. Technol.*, vol. 87, pp. 42–50, Jan. 2014.
[18] S. Kim and T. F. Schatzki, "Apple watercore sorting system using X-ray imagery: I. algorithm development," *Trans. ASAE*, vol. 43, no. 6, pp. 1695–1702, 2000.
[19] A. M.-Herreros, M.-A. M.-García, A. Blanco, J. Val, M. E. F.-Valle, and P. Barreiro, "Assessment of watercore development in apples with MRI: Effect of fruit location in the canopy," *Postharvest Biol. Technol.*, vol. 86, pp. 125–133, Dec. 2013.
[20] P. Barreiro, J. R.–Cabello, M. E. F.-Valle, C. Ortiz, and M. R.-Altisent, "Mealiness assessment in Apples using MRI techniques," *Magn. Reson. Imag.*, vol. 17, no. 2, pp. 275–281, Feb. 1999.
[21] R. Simons, "The morphological and anatomical characteristics of watercore in apples," *Proc. Amer. Soc. Horticultural Sci.*, vol. 93, pp. 762–774, 1968.
[22] W. J. Bramlage and M. R. Shipway, "Loss of watercore and development of internal breakdown during storage of 'delicious' apples, as determined by repeated light transmittance measurements of intact apples," *Proc. Amer. Soc. Horticultural Sci.*, vol. 90, pp. 475–483, 1967.
[23] T. Sun, S. Song, Y. Yao, and M. Tian, "Measures for reducing apple water core disorder," China Fruits, no. 2, 2000.
[24] A. Itai, "Watercore in Fruits," in *Abiotic Stress Biology in Horticultural Plants*. Tokyo, Japan: Springer, 2015, pp. 127–145.
[25] F. Tanaka, F. Hayakawa, and M. Tatsuki, "Flavor and texture characteristics of 'Fuji' and related apple (malus domestica l.) cultivars, focusing on the rich watercore," *Molecules*, vol. 25, no. 5, Mar. 2020, Art. no. 1114.
[26] D. E. Khaled, N. Novas, J. A. Gazquez, R. M. Garcia, and F. M.-Agugliaro, "Fruit and vegetable quality assessment via dielectric sensing," *Sensors*, vol. 15, no. 7, pp. 15 363–15 397, Jun. 2015.
[27] J.-C. Chiao, S. Bing, and K. Chawang, "Review on noninvasive radio-frequency sensing for closed-loop body health management," in *Proc. IEEE Int. Symp. Radio- Freq. Integration Technol.*, 2021, pp. 1–3.
[28] M. P. Robinson, J. Clegg, and D. A. Stone, "A novel method of studying total body water content using a resonant cavity: Experiments and numerical simulation," *Phys. Med. Biol.*, vol. 48, no. 1, pp. 113–125, Jan. 2003.
[29] D. A. Stone and M. P. Robinsons, "Total body water content observations using cavity-perturbation techniques," in *Proc. High Freq. Postgraduate Student Colloq.*, 2003, pp. 31–34.
[30] A. W. Kraszewski, S. O. Nelson, and T. S. You, "Use of a microwave cavity for sensing dielectric properties of arbitrarily shaped biological objects," *IEEE Trans. Microw. Theory Techn.*, vol. 38, no. 7, pp. 858–863, Jul. 1990.
[31] J.-C. Chiao et al., "Applications of microwaves in medicine," *IEEE J. Microw.*, vol. 3, no. 1, pp. 134–169, Jan. 2023.
[32] K. Aydin, I. Bulu, K. Guven, M. Kafesaki, C. M. Soukoulis, and E. Ozbay, "Investigation of magnetic resonances for different split-ring resonator parameters and designs," *New J. Phys.*, vol. 7, no. 1, 2005, Art. no. 168.
[33] M. Baghelani, Z. Abbasi, M. Daneshmand, and P. E. Light, "Non-invasive continuous-time glucose monitoring system using a chipless printable sensor based on split ring microwave resonators," *Sci. Rep.*, vol. 10, no. 1, Jul. 2020, Art. no. 12980.
[34] G. Ekinci, A. Calikoglu, S. N. Solak, A. D. Yalcinkaya, G. Dundar, and H. Torun, "Split-ring resonator-based sensors on flexible substrates for glaucoma monitoring," *Sensors Actuators A: Phys.*, vol. 268, pp. 32–37, 2017.
[35] H. Choi et al., "Design and in vitro interference test of microwave non-invasive blood glucose monitoring sensor," *IEEE Trans. Microw. Theory Techn.*, vol. 63, no. 10, pp. 3016–3025, Oct. 2015.
[36] J. Kilpijärvi, J. Tolvanen, J. Juuti, N. Halonen, and J. Hannu, "A non-invasive method for hydration status measurement with a microwave sensor using skin phantoms," *IEEE Sensors J.*, vol. 20, no. 2, pp. 1095–1104, Jan. 2020.
[37] S. Bing, K. Chawang, and J.-C. Chiao, "A self-tuned method for impedance-matching of planar-loop resonators in conformable wearables," *Electronics*, vol. 11, no. 17, Jan. 2022, Art. no. 2784.
[38] J. Wei, "Distributed capacitance of planar electrodes in optic and acoustic surface wave devices," *IEEE J. Quantum Electron.*, vol. 13, no. 4, pp. 152–158, Apr. 1977.
[39] F. Maradei and S. Caniggia, *Appendix A: Formulae for Partial Inductance Calculation* Chichester, U.K.: Wiley, 2008, pp. 481–486.
[40] S. Bing, K. Chawang, and J.-C. Chiao, "A flexible tuned radio-frequency planar resonant loop for noninvasive hydration sensing," *IEEE J. Microw.*, vol. 3, no. 1, pp. 181–192, Jan. 2023.
[41] S. Bing, K. Chawang, and J. C. Chiao, "A radio-frequency planar resonant loop for noninvasive monitoring of water content," in *Proc. IEEE Sensors*, 2022, pp. 1–4.
[42] G. Niu, S. Bing, B. Zhang, and J.-C. Chiao, "Particle filter based diagnosis and prognosis for human hydration states," *IEEE Sens. Lett.*, vol. 7, no. 9, pp. 1–4, Sep. 2023.
[43] S. Bing, K. Chawang, and J.-C. Chiao, "A resonant coupler for subcutaneous implant," *Sensors*, vol. 21, no. 23, Dec. 2021, Art. no. 8141.
[44] S. Bing, K. Chawang, and J. C. Chiao, "A tuned microwave resonant system for subcutaneous imaging," *Sensors*, vol. 23, no. 6, Mar. 2023, Art. no. 3090.
[45] S. Bing and J.-C. Chiao, "A planar conformal microwave resonator for subcutaneous imaging," in *Proc. IEEE Int. Symp. Antennas Propag. USNC-URSI Radio Sci. Meeting*, 2023, pp. 335–336.
[46] S. Bing, K. Chawang, and J.-C. Chiao, "A tuned microwave resonant sensor for skin cancerous tumor diagnosis," *IEEE J. Electromagnetics, RF Microw. Med. Biol.*, vol. 7, no. 4, pp. 320–327, Dec. 2023.
[47] S. Bing, K. Chawang, and J. C. Chiao, "Resonant coupler designs for subcutaneous implants," in *Proc. IEEE Wireless Power Transfer Conf.*, 2021, pp. 1–4.
[48] USDA, "Fresh apples, grapes, and pears: World markets and trade," Economics, Statistics and Market Information System, U.S. Department of Agriculture (USDA), Washington, D.C., USA, Tech. Rep., Jun. 2023.
[49] J. E. Storer, "Impedance of thin-wire loop antennas," *Trans. Amer. Inst. Elect. Engineers. Part 1. Commun. Electron.*, vol. 75, no. 5, pp. 606–619, Nov. 1956.
[50] S. Kumar and P. C. Sharma, "Process protocol for mechanical separation of fruit core and seeds from apple fruits," *Int. J. Farm Sci.*, vol. 7, no. 1, pp. 147–153, 2017.
[51] G. C. Marlow and W. H. Loescher, "Watercore," *Horticultural Rev.*, vol. 6, pp. 189–251, 1984.
[52] S. Kasai and O. Arakawa, "Antioxidant levels in watercore tissue in 'Fuji' apples during storage," *Postharvest Biol. Technol.*, vol. 55, no. 2, pp. 103–107, Feb. 2010.
[53] Z. Gao, S. Jayanty, R. Beaudry, and W. Loescher, "Sorbitol transporter expression in apple sink tissues: Implications for fruit sugar accumulation and watercore development," *J. Amer. Soc. Horticultural Sci.*, vol. 130, no. 2, pp. 261–268, Mar. 2005.
[54] D. F. Fisher, C. P. Harley, and C. Brooks, "The influence of temperature on the development of watercore," in *Proc. Amer. Soc. Hort. Sci.*, vol. 27, 1931, pp. 276–280.
[55] H. Yamada, H. Ohmura, C. Arai, and M. Terui, "Effect of preharvest fruit temperature on ripening, sugars, and watercore occurrence in apples," *J. Amer. Soc. Horticultural Sci.*, vol. 119, no. 6, pp. 1208–1214, Nov. 1994.
[56] M. W. Williams and H. D. Billingsley, "Watercore development in apple fruits as related to sorbitol levels in the tree sap and to minimum temperatures," *J. Amer. Soc. Horticultural Sci.*, vol. 98, pp. 205–207, 1973.
[57] T. Tomana and H. Yamada, "Relationship between temperature and fruit quality of apple cultivars grown at different locations," *Engei Gakkai zasshi*, vol. 56, no. 4, pp. 391–397, 1988.
[58] Y. Zhang, Z. Wang, X. Tian, X. Yang, Z. Cai, and J. Li, "Online analysis of watercore apples by considering different speeds and orientations based on VIS/NIR full-transmittance spectroscopy," *Infrared Phys. Technol.*, vol. 122, May 2022, Art. no. 104090.
[59] C. Han, Y. Jifan, T. Hao, Y. Jinshan, and X. Huirong, "Evaluation of the optical layout and sample size on online detection of apple watercore and SSC using VIS/NIR spectroscopy," *J. Food Comp. Anal.*, vol. 123, Oct. 2023, Art. no. 105528.

[60] Z. Guo et al., "Quantitative detection of apple watercore and soluble solids content by near infrared transmittance spectroscopy," *J. Food Eng.*, vol. 279, Aug. 2020, Art. no. 109955.
[61] P. Baranowski, J. Lipecki, W. Mazurek, and R. T. Walczak, "Detection of watercore in 'Gloster' apples using thermography," *Postharvest Biol. Technol.*, vol. 47, no. 3, pp. 358–366, Mar. 2008.
[62] J. Li, X. Tian, W. Huang, B. Zhang, and S. Fan, "Application of long-wave near infrared hyperspectral imaging for measurement of soluble solid content (SSC) in pear," *Food Anal. Methods*, vol. 9, no. 11, pp. 3087–3098, Nov. 2016.
[63] R. Wang, D. Wang, X. Ren, and H. Ma, "Nondestructive detection of apple watercore disease based on electric features," *Trans. Chin. Soc. Agricultural Eng.*, vol. 34, no. 5, pp. 129–136, 2018.
[64] S. A. Jennings, A.-K. Koehler, K. J. Nicklin, C. Deva, S. M. Sait, and A. J. Challinor, "Global potato yields increase under climate change with adaptation and CO_2 fertilisation," *Front. Sustain. Food Syst.*, vol. 4, Dec. 2020, Art. no. 519324.
[65] IMARC, "Potato chips market: Global industry trends, share, size, growth, opportunity and forecast 2023-2028," IMARC Group, Noida, India, Tech. Rep., May 2023. [Online]. Available: https://www.imarcgroup.com/potato-chips-manufacturing-plant
[66] U.N.E.C., "Food loss and waste–the case of seed potato certification," United Nations Economic Commission for Europe, (U. N. E.C.)., Geneva, Switzerland, Tech. Rep., Jun. 2017. [Online]. Available: https://unece.org/fileadmin/DAM/trade/agr/meetings/ge.06/2017/RapporteursMtg_TheNetherlands/Food_Loss_Waste.pdf
[67] P. Muruganantham, N. H. Samrat, N. Islam, J. Johnson, S. Wibowo, and S. Grandhi, "Rapid estimation of moisture content in unpeeled potato tubers using hyperspectral imaging," *Appl. Sci.*, vol. 13, no. 1, Jan. 2023, Art. no. 53.
[68] G. Cruz et al., "Impact of pre-drying and frying time on physical properties and sensorial acceptability of fried potato chips," *J. Food Sci. Technol.*, vol. 55, no. 1, pp. 138–144, Jan. 2018.
[69] T. Zhang, J. Li, Z. Ding, and L. Fan, "Effects of initial moisture content on the oil absorption behavior of potato chips during frying process," *Food Bioprocess Technol.*, vol. 9, no. 2, pp. 331–340, Feb. 2016.
[70] E. Ağçam, "Modeling of the changes in some physical and chemical quality attributes of potato chips during frying process," *Appl. Food Res.*, vol. 2, no. 1, Jun. 2022, Art. no. 100064.
[71] A. Odenigbo, J. Rahimi, M. Ngadi, D. Wees, A. Mustafa, and P. Seguin, "Quality changes in different cultivars of sweet potato during deep-fat frying," *J. Food Process. Technol.*, vol. 3, no. 5, pp. 1–6, 2012.
[72] A. Kaur, N. Singh, and R. Ezekiel, "Quality parameters of potato chips from different potato cultivars: Effect of prior storage and frying temperatures," *Int. J. Food Properties*, vol. 11, no. 4, pp. 791–803, Nov. 2008.
[73] M. K. Krokida, V. Oreopoulou, and Z. B. Maroulis, "Water loss and oil uptake as a function of frying time," *J. Food Eng.*, vol. 44, no. 1, pp. 39–46, 2000.
[74] C. E. Onu, P. K. Igbokwe, J. T. Nwabanne, C. O. Nwajinka, and P. E. Ohale, "Evaluation of optimization techniques in predicting optimum moisture content reduction in drying potato slices," *Artif. Intell. Agriculture*, vol. 4, pp. 39–47, 2020.
[75] M. Eltawil, D. Samuel, and O. Singhal, "Potato storage technology and store design aspects," *Agricultural Eng. Int.*, vol. 08, no. 11, pp. 1–18, 2006.
[76] J. Dong and W. Guo, "Nondestructive determination of apple internal qualities using near-infrared hyperspectral reflectance imaging," *Food Anal. Methods*, vol. 8, no. 10, pp. 2635–2646, Nov. 2015.

Sen Bing (Member, IEEE) received the B.Tech. degree in electronics and information science and technology from Hainan Normal University, Haikou, China, in 2017, and the M.S. degree in electrical engineering in 2019 from Southern Methodist University, Dallas, TX, USA, where he is currently working toward the Ph.D. degree in electrical and computer engineering.

He has authored five journal articles, seven conference papers, and co-authored two journal articles on optimizing performance for microwave biomedical sensors and implants. He has co-authored four journal articles and four conference papers on factors affecting pH performance, and authored one conference paper on low-cost ultrasound medical imaging. His research interests include microwave biomedical devices, electrochemical biosensors, wearable electronics, medical imaging, and RF devices.

Khengdauliu Chawang (Graduate Student Member, IEEE) received the bachelor of technology degree in electronics and communication engineering from the National Institute of Technology Nagaland, Dimapur, Nagaland, India, in 2012, the master of science degree in electrical engineering from the University of Texas at Arlington, Arlington, TX, USA, in 2019. She is currently working toward the Ph.D. degree with the Department of Electrical and Computer Engineering, Southern Methodist University, Dallas, TX.

She has authored/coauthored seven conference papers on factors affecting pH performance. Her research interest focuses on flexible and ultraflexible devices by micro and nano fabrication, electro-chemical biosensors, wearable electronics, and RF devices.

Jung-Chih Chiao (Fellow, IEEE) received the B.S. degree in electrical engineering from the Electrical Engineering Department, National Taiwan University, Taipei, Taiwan, in 1988, the M.S. and Ph.D. degrees in electrical engineering from the California Institute of Technology, Pasadena, CA, USA, in 1991 and 1995, respectively.

From 2002 to 2018, he was Janet and Mike Greene endowed Professor and Jenkins Garrett Professor of electrical engineering with the University of Texas–Arlington. He was a Research Scientist with the Optical Networking Systems and Testbeds Group at Bell Communications Research, an Assistant Professor of electrical engineering with the University of Hawaii, Manoa, and a Product Line Manager and Senior Technology Advisor with Chorum Technologies. He is currently Mary and Richard Templeton Centennial Chair Professor in electrical and computer engineering with Southern Methodist University (SMU), Dallas, TX, USA. He has authored or coauthored and edited numerous peer-reviewed technical journal and conference papers, book chapters, proceedings, and books. He holds 20 patents in RF MEMS, MEMS optical, liquid crystal, nano-scale fabrication, and wireless medical sensor technologies.

Dr. Chiao has been a Chair and Technical Program Chair of several international conferences, including 2018 IEEE International Microwave Biomedical Conference (IMBioC) and 2021 IEEE Wireless Power Transfer Conference. He was the Chair for the IEEE MTT-S Technical Committee 10 "Biological Effect and Medical Applications of RF and Microwave," and an Associate Editor for IEEE TRANSACTIONS ON MICROWAVE THEORY AND TECHNIQUES. He was the founding Editor-in-Chief for IEEE JOURNAL OF ELECTROMAGNETICS, RF, AND MICROWAVES IN MEDICINE AND BIOLOGY. He is with the Editorial Board of IEEE ACCESS and Track Editor for IEEE JOURNAL OF MICROWAVES. His research works have been covered by media extensively, including Forbes, National Geographic magazine, National Public Radio, and CBS Henry Ford Innovation Nation. He was the recipient of Lockheed Martin Aeronautics Company Excellence in Engineering Teaching Award; Tech Titans Technology Innovator Award; Research in Medicine award in the Heroes of Healthcare; IEEE Region 5 Outstanding Engineering Educator award; IEEE Region 5 Excellent Performance award; 2012–2014 IEEE MTT Distinguished Microwave Lecturer; 2017–2019 IEEE Sensors Council Distinguished Lecturer; Pan Wen-Yuan Foundation Excellence in Research Award; and the 2011 Edith and Peter O'Donnell Award in Engineering by The Academy of Medicine, Engineering and Science of Texas. He is a Fellow of IET, SPIE, and AIMBE.